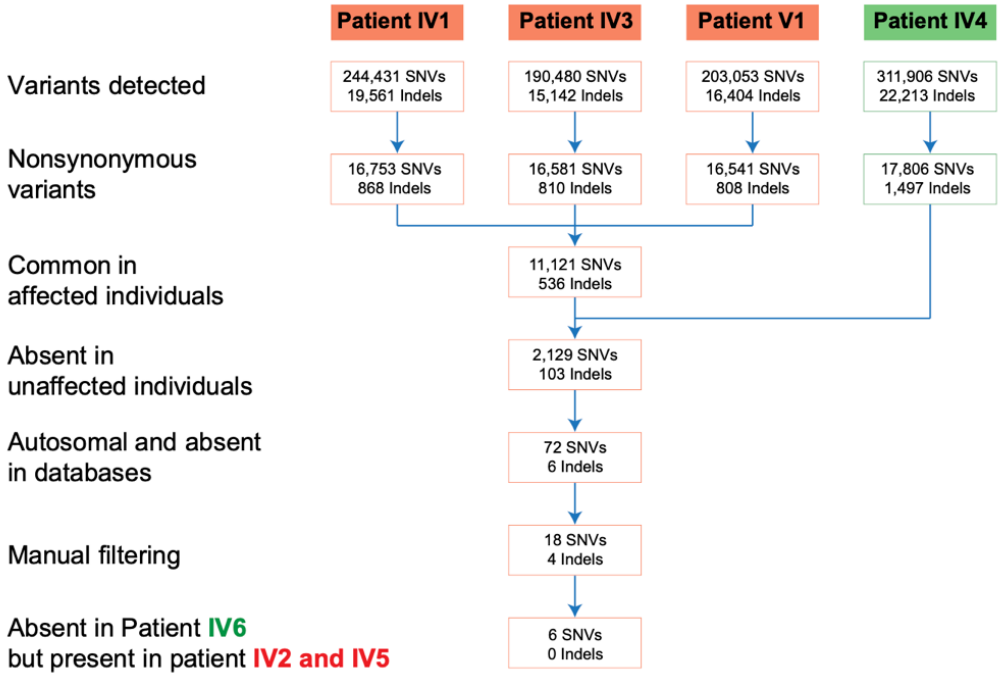

Supplementary Figure 1 – Filtering of single nucleotide variants (SNVs) to identify MSP-associated candidate genes.

The filtering paradigm used to detect novel sequence variants that co-segregated with disease is shown. Affected patients are represented by red and unaffected patients by green.

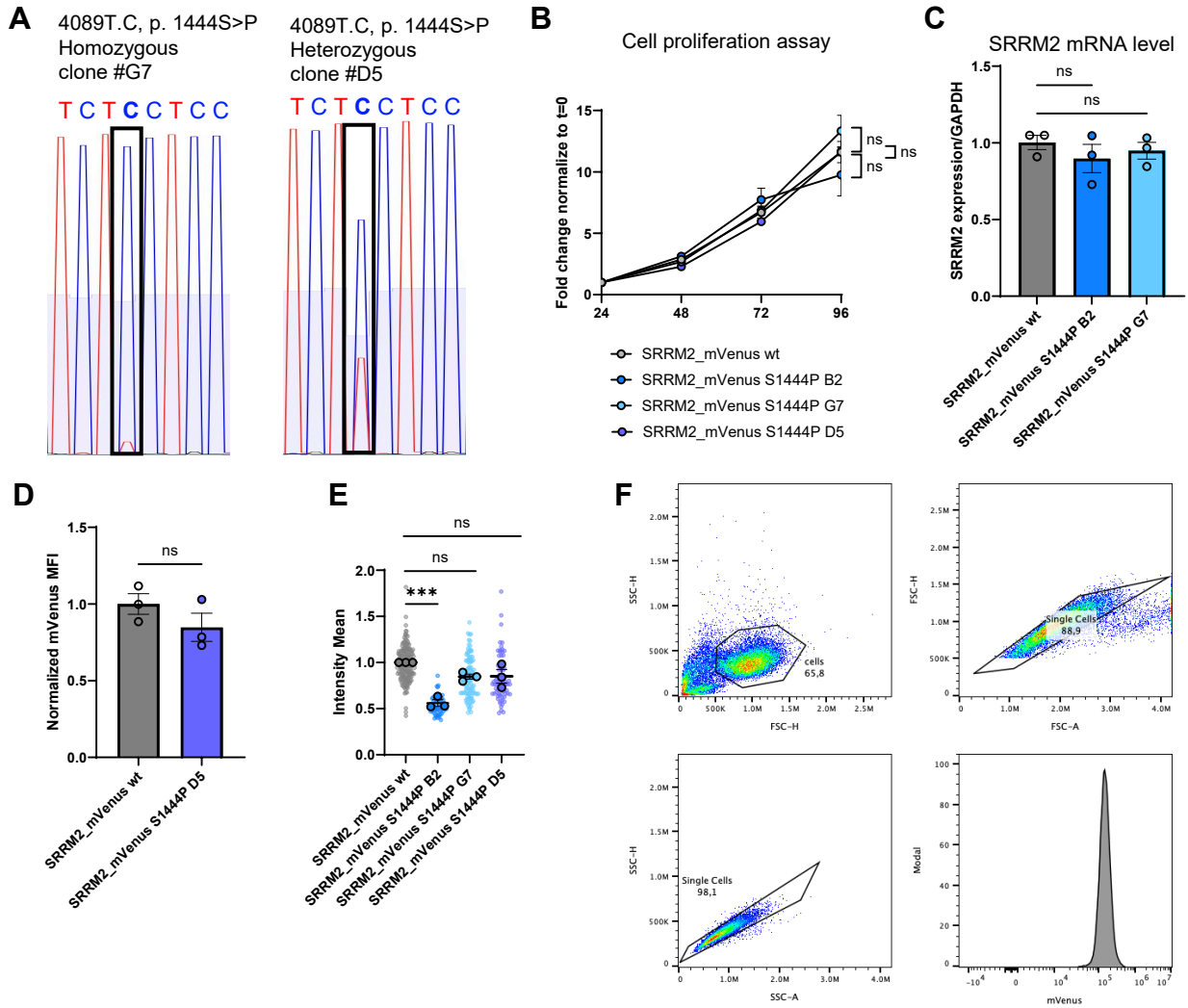

Supplementary Figure 2 – Characterization of SRRM2 S1444P model cell lines.

(**A**) Nanopore sequencing confirmation of homozygous (G7) and heterozygous (D5) SRRM2 c.4089T.C (S1444P) cell lines. (**B**) Cell proliferation measured by Alamar Blue fluorescence showed no significant difference between WT and mutant S1444P cells. (**C**) qPCR assessment of SRRM2 mRNA levels following gene editing. (**D**) Flow cytometry to quantify SRRM2 protein levels in S1444P heterozygous (D5) cell line. (**E**) SRRM2-mVenus signal in WT and mutant S1444P cells quantified using Imaris software. (**F**) Representative gating scheme used for flow cytometry analysis. Cells were first gated on FSC-H versus SSC-H to exclude debris, followed by doublet exclusion using FSC-H/FSC-A and SSC-H/SSC-A. mVenus MFI was quantified from the resulting singlet population in the appropriate channel. FSC: forward scatter; SSC: side scatter; H: height; A: area; MFI: mean fluorescence intensity

(**B-E**): Different cell passages were used as replicates. **B**. n=3, 3, 3, 3. **C**. n=3, 3, 3. **D**. n=3, 3. **E**. n=3, 3, 3, 3 with individual cells per replicate shown as dots. One-way ANOVA was used for **B**, **C**, and **E**. Unpaired two-tailed t-test was used for **D**. ns=p>0.05, *p<0.05, **p<0.01, ***p<0.001, ****p<0.0001.

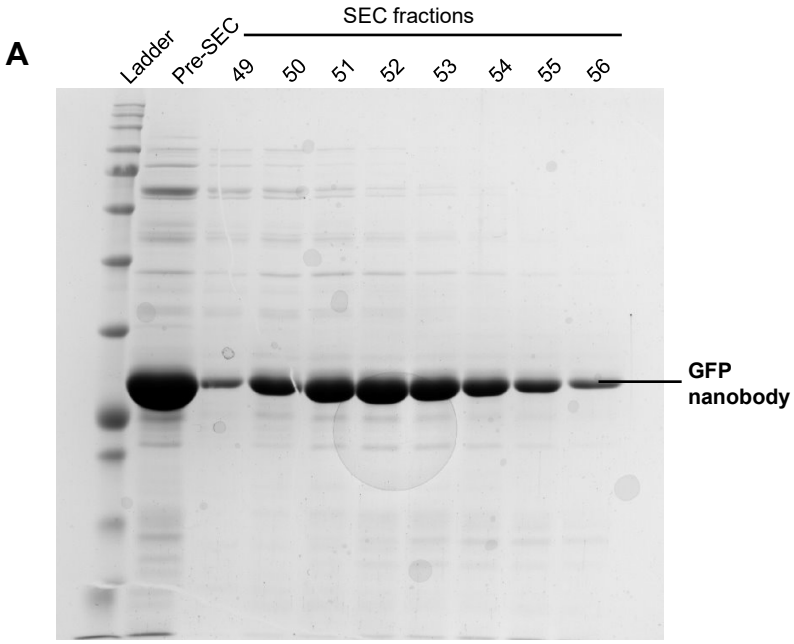

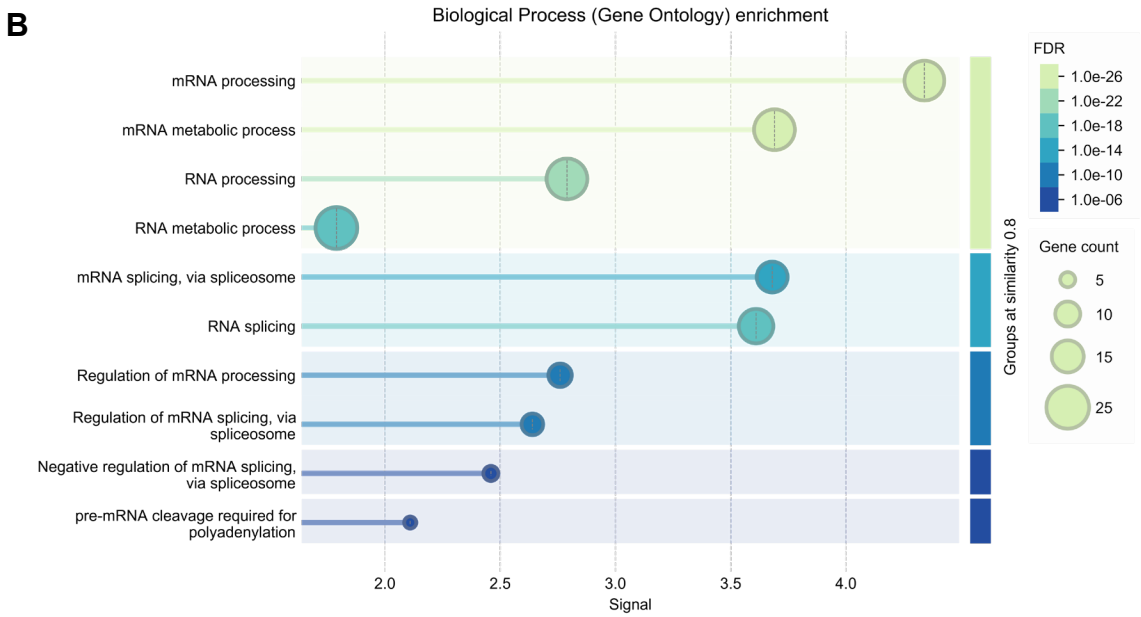

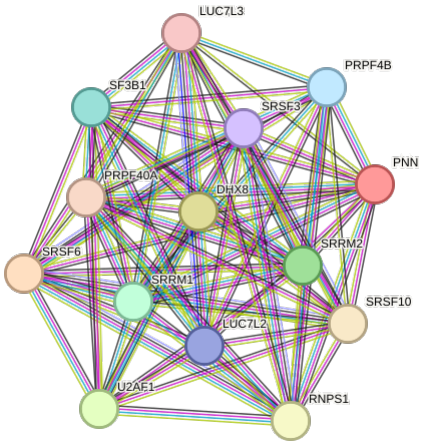

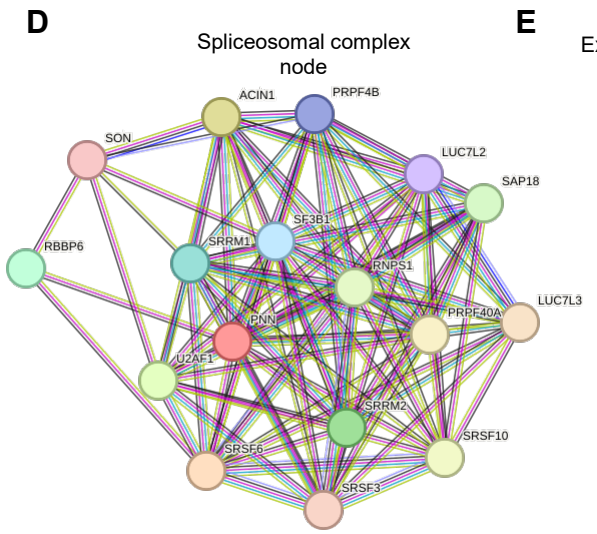

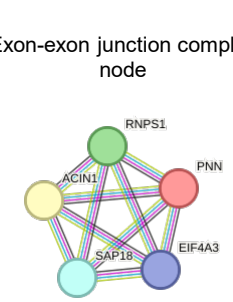

Supp Figures 3

Supplementary Figure 3 – SRRM2 wt and S1444P interactome analysis

(**A**) SDS-PAGE confirming purification of the GFP-nanobody, which was subsequently used for enrichment of SRRM2_mVenus. SEC: size exclusion chromatography. (**B**) Enrichment analysis of the SRRM2 wt proteome confirming that the majority of SRRM2 interactors were nuclear speckle proteins and/or associated with mRNA processing. (**C-E**). Nodes displaying proteins associated with different complexes in the SRRM2 interactome.

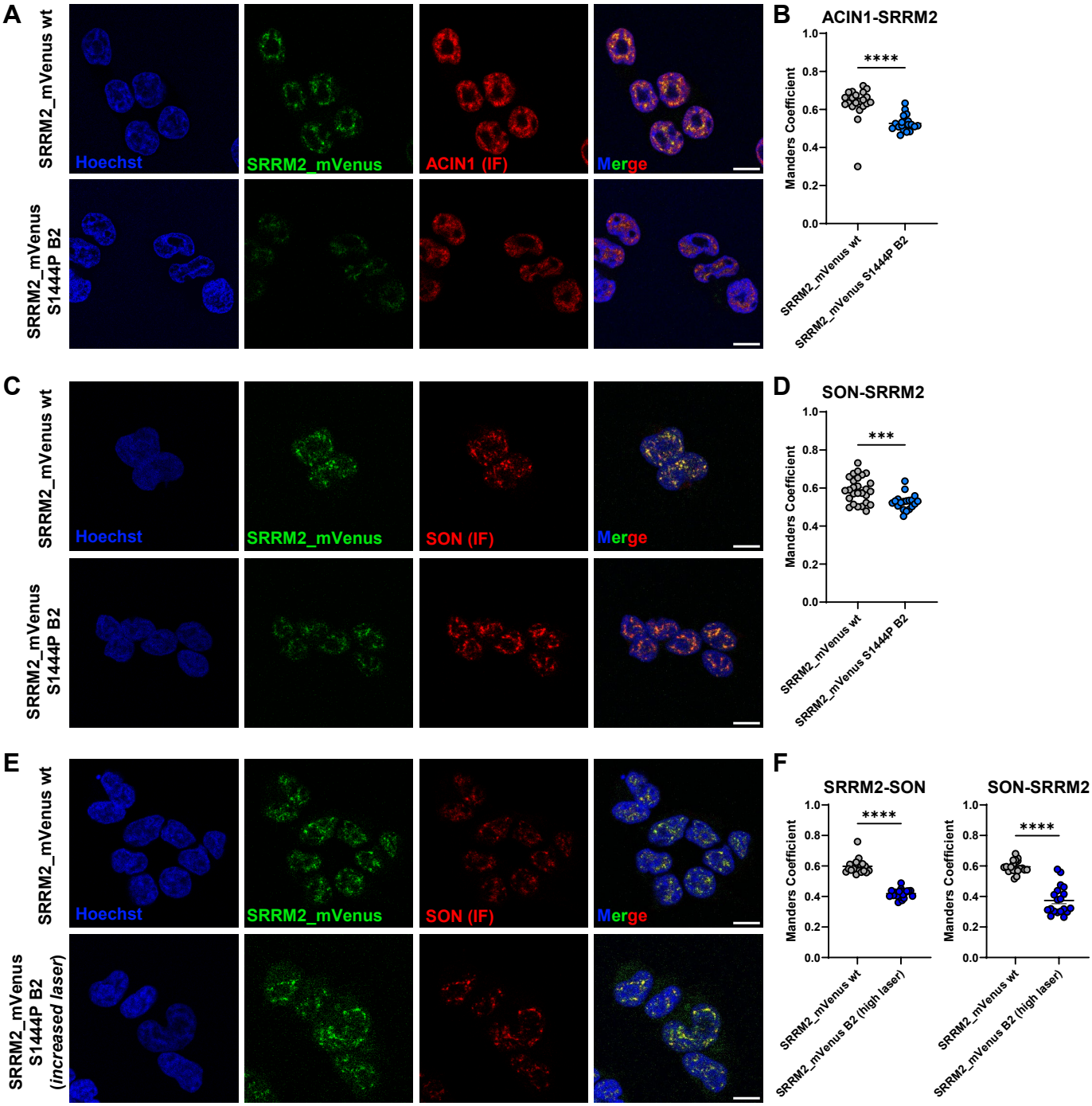

Supp Figures 4

Supplementary Figure 4 – Additional analysis on SRRM2 protein-protein interaction in SRRM2 mVenus wt and S1444P B2 cells

(**A**) Additional representative images used to assess SRRM2 and ACIN1 colocalization. SRRM2 is imaged through fusion to the fluorescent protein mVenus, ACIN1 is visualized through immunofluorescence. (**B**) Manders coefficient of ACIN1 with SRRM2. (**C**) Additional representative images of SRRM2 and SON colocalization. SRRM2 is imaged through fusion to the fluorescent protein mVenus, SON is visualized through immunofluorescence. (**D**) Manders coefficient of SON with SRRM2. (**E**) Representative confocal images of wt and S1444P B2 cells expressing SRRM2-mVenus. To facilitate comparison of protein colocalization, mutant cells were imaged using increased laser intensity to achieve signal levels comparable to WT. (**F**) Manders coefficient of SRRM2 and SON.

(**A, C**) Different cell passages were used as replicates. Images are representatives of three replicates. (**E**) One replicate was imaged and quantified. (**B, D, F**): Individual cells per replicate are shown as dots. **B**. n=21, 20. **D**. n=27, 19. **F**. n=20, 19. Unpaired, two-tailed t-test. ns=p>0.05, *p<0.05, **p<0.01, ***p<0.001, ****p<0.0001.

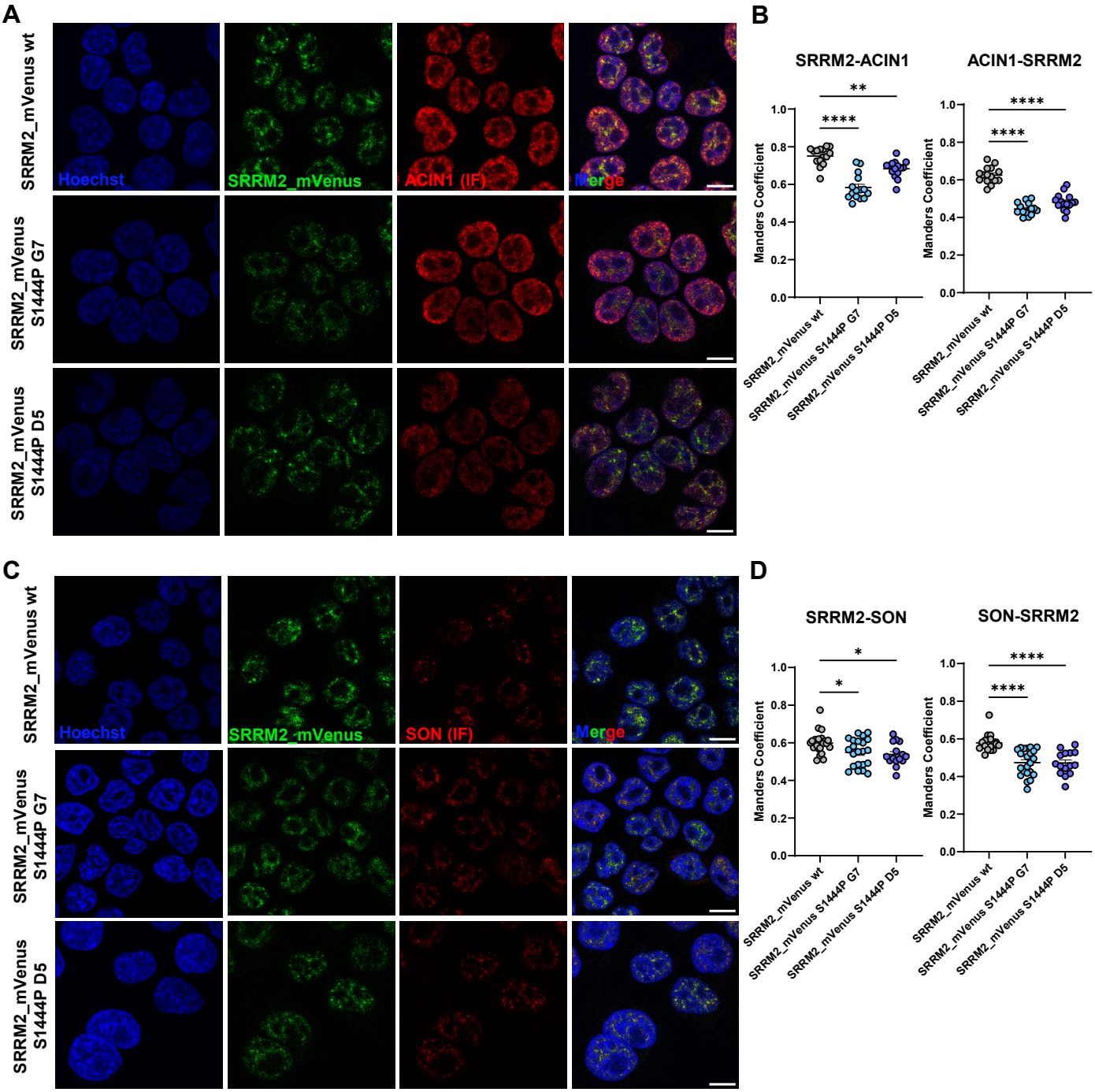

Supplementary Figure 5 – Analysis on SRRM2 protein-protein interaction in SRRM2 mVenus wt and other additional S1444P clones

(**A**) Immunofluorescence of ACIN1 and SRRM2 in SRRM2 wt and S1444P G7 (homozygous) and D5 (heterozygous) cells. (**B**) Manders coefficient of ACIN1 and SRRM2. (**C**) Immunofluorescence of SON and SRRM2 in SRRM2 wt and S1444P G7 (homozygous) and D5 (heterozygous) cells. (**D**) Manders coefficient of SON and SRRM2.

(**A-D**) Different cell passages were used as replicates. Images are representatives of three replicates. (**B, D**) Individual cells per replicate are shown as dots. **B**. n=15, 15, 15. **D**. n=15, 15, 15. One-way ANOVA. *p<0.05. **p<0.01, ****p<0.0001.

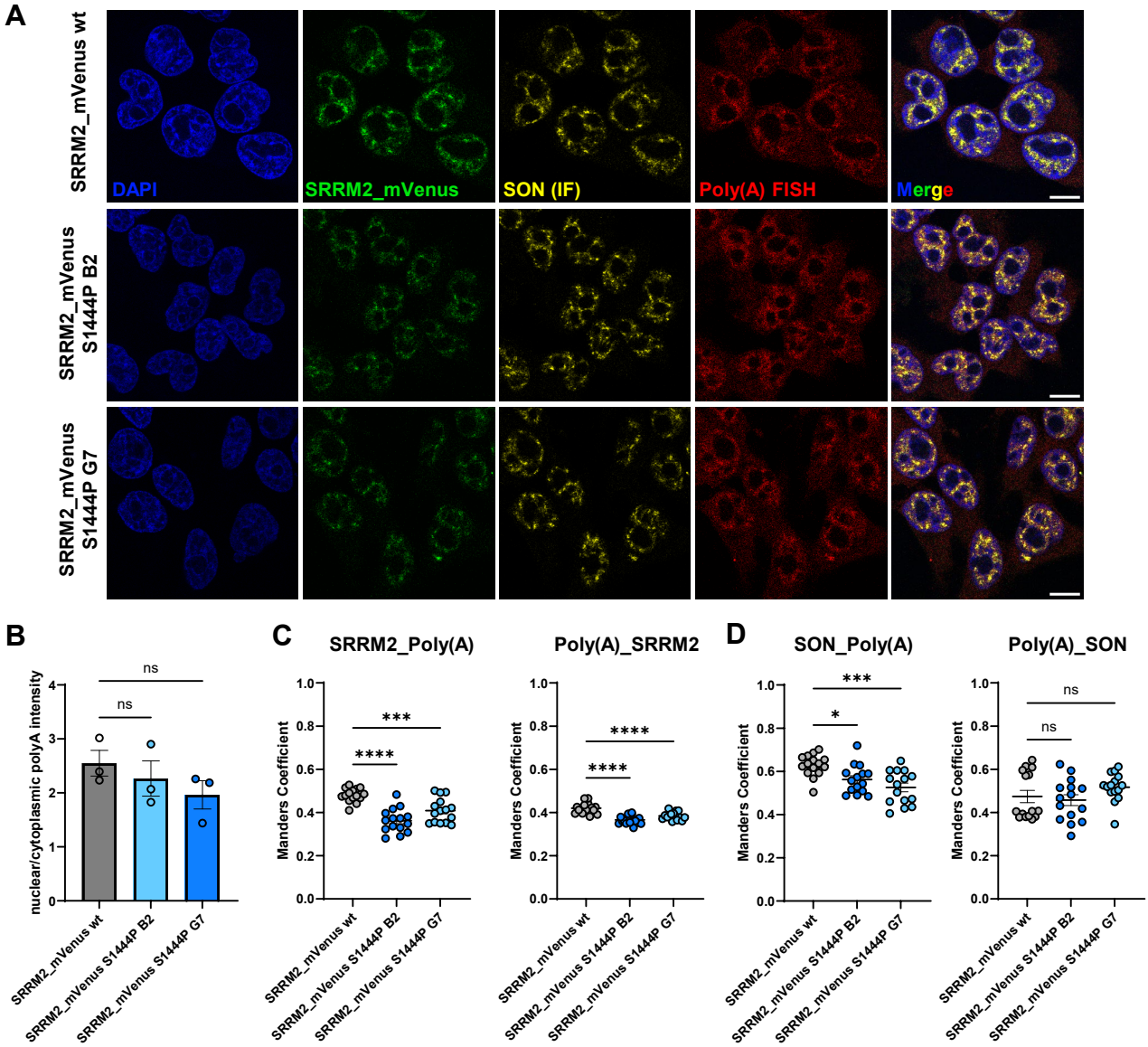

Supplementary Figure 6 – Analysis of nuclear speckle cohesion in SRRM2 mVenus wt and S1444P mutant cells using poly(A) FISH

(**A**) Additional confocal images of WT and mutant S1444P cells subjected to poly(A) FISH (red) and immunofluorescence staining for SON (yellow). (**B**) Quantification of nuclear versus cytoplasmic poly(A) RNA signal intensity was performed using Imaris software, with the nuclear compartment defined by DAPI masking. (**C**) Manders coefficient of poly(A) signal and SRRM2. (**D**) Manders coefficient of poly(A) signal and SON.

(**A-D**) Different cell passages were used as replicates. Images are representatives of three replicates. (**B-D**) Individual cells per replicate are shown as dots. **C**. n=15, 15, 15. **D**. n=15, 15, 15. One-way ANOVA. ns=p>0.05, *p<0.05, ***p<0.001, ****p<0.0001.

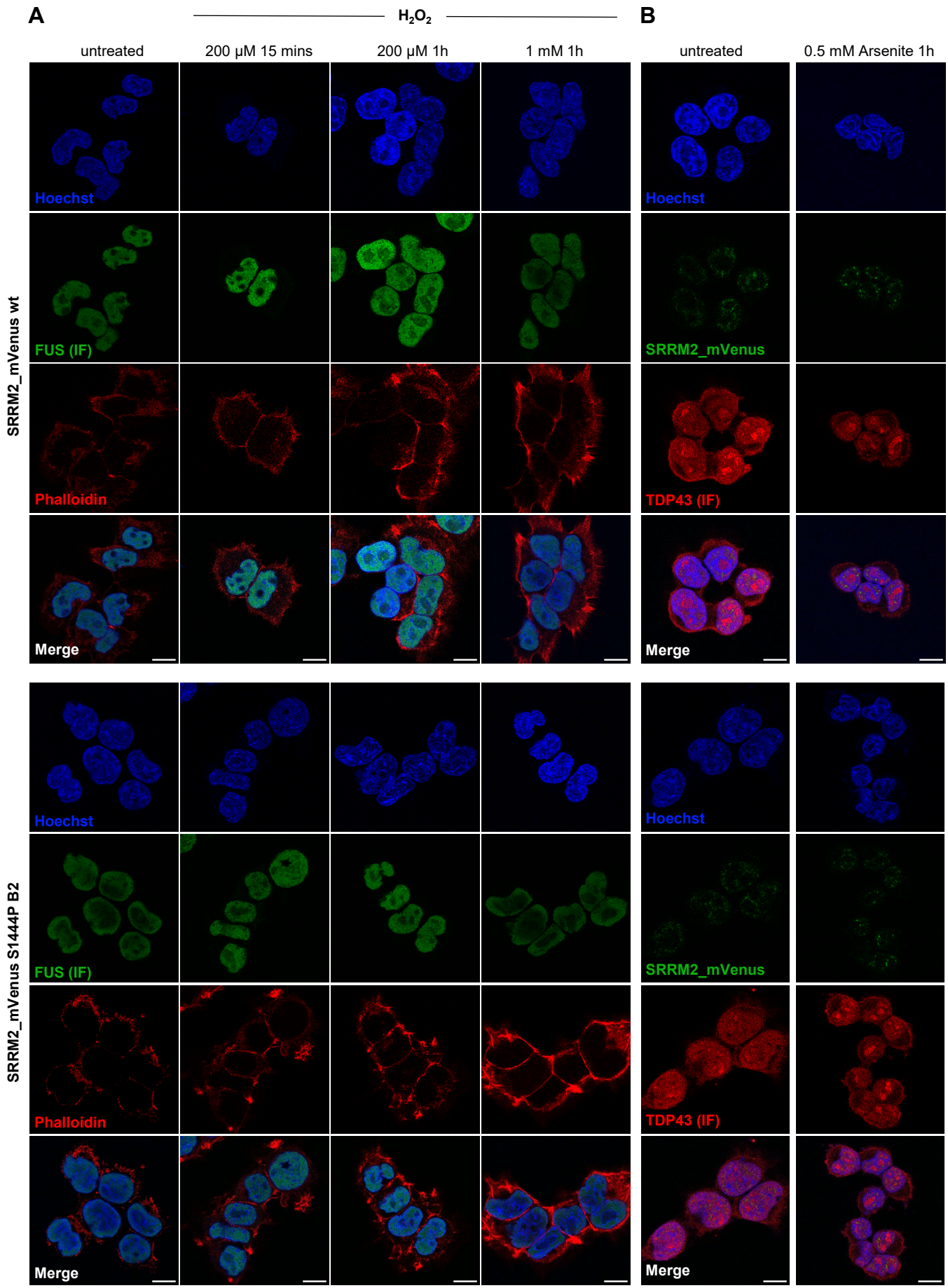

Supp Figures 7

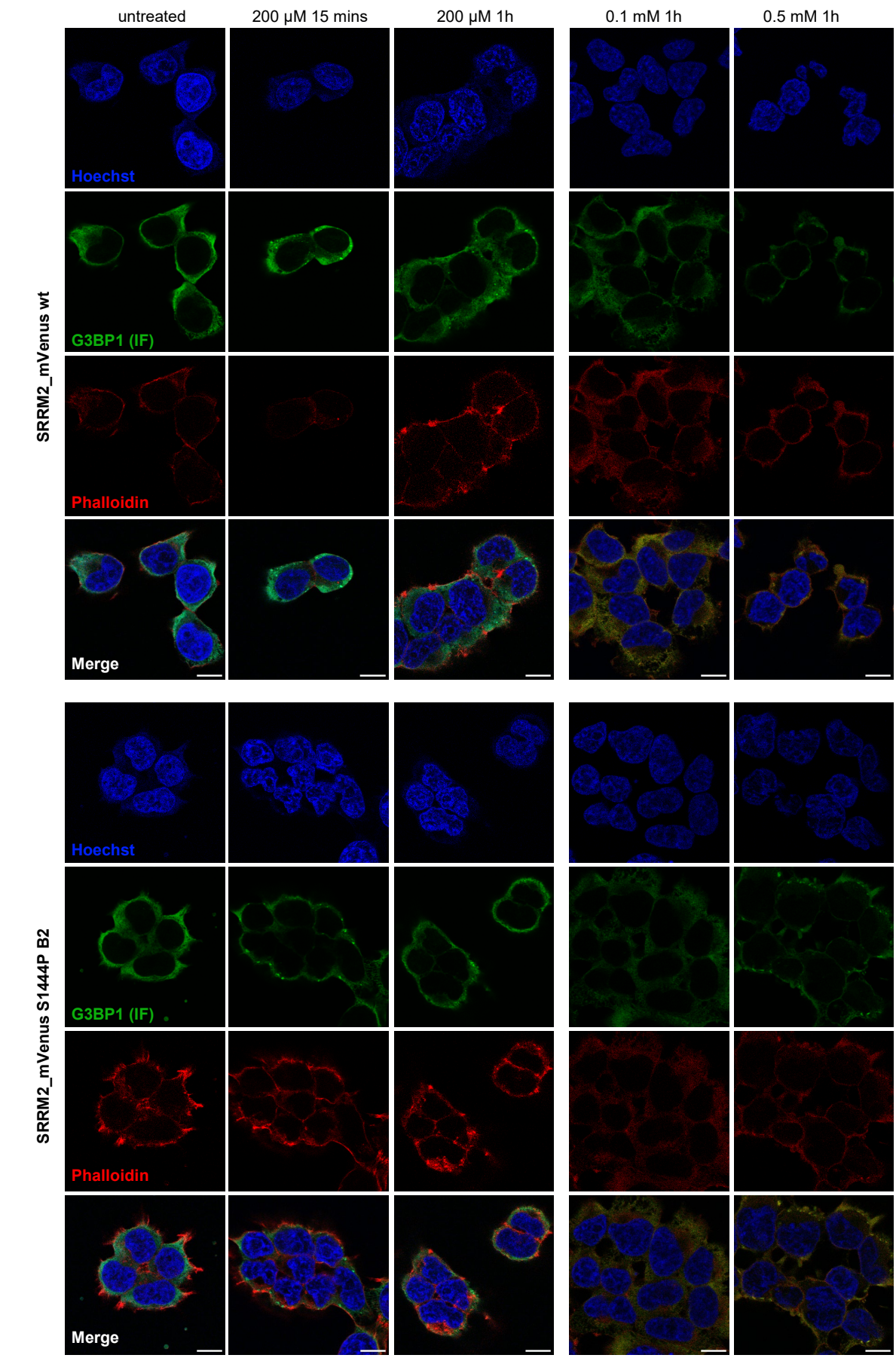
C
H2O2
Sodium arsenite
untreated
200 µM 15 mins
200 µM 1h
0.1 mM 1h
0.5 mM 1h
SRRM2_mVenus wt
SRRM2_mVenus S1444P B2
Hoechst
G3BP1 (IF)
Phalloidin
Merge

Supplementary Figure 7 – Analysis of stress granule formation in S1444P cells under oxidative stress.

(**A**) FUS immunofluorescence to monitor FUS nuclear export and cytoplasmic aggregation in S1444P cells. Cytoplasmic localization was not observed in wt or S1444P cells. (**B**) TDP43 immunofluorescence to assess TDP43 mislocalization in S1444P cells. TDP43 localization was comparable between wt and S1444P cells. (**C**) G3BP1 immunofluorescence indicating stress granule formation in wt and S1444P cells. G3BP1 granule formation was unchanged between wt and S1444P cells but responsive to varying concentrations of stressors.

(**A-C**) Different cell passages were used as replicates. Images are representatives of two biological replicates. Hoechst labels DNA in nuclei, phalloidin binds F-actin and is used here to indicate cell boundaries.

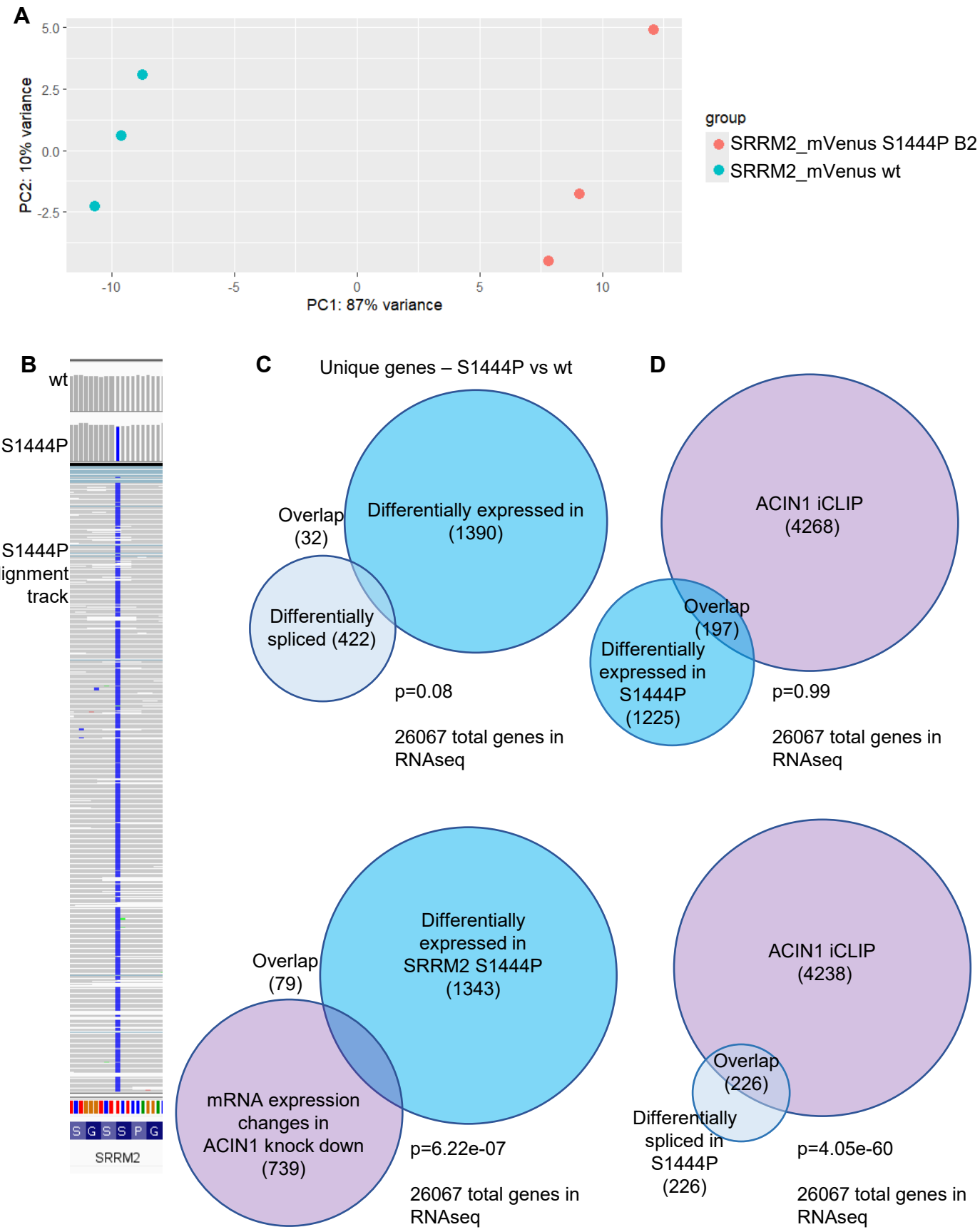

Supp Figures 8

Supplementary Figure 8 – Characterization of SRRM2 S1444P model cell lines.

(**A**) PCA plot showing distinct differences between wt and S1444P transcriptomes. (**B**) RNA-seq alignment tracks of the SRRM2 locus confirm the S1444P substitution. (**C)** Comparison between differentially expressed and differentially spliced genes in SRRM2 S1444P vs wt cells. (**D**) Upper right: Venn diagram showing the overlap between genes differentially expressed in SRRM2 S1444P mutant cells compared to wt and introns bound by ACIN1. Lower right: Venn diagram showing the overlap between differentially spliced genes and introns bound by ACIN1. Lower left: Venn diagram showing the overlap between differentially expressed genes in SRRM2 S1444P compared to wt and differentially expressed genes in siACIN1 cells. All ACIN1 data sets (iCLIP and siACIN1 RNAseq) were obtained from Rodor et al., 2016. Only genes enriched under all three ACIN1 variant conditions in Roder et al. were used for comparison. Hypergeometric testing was performed in R.

(**A-D**) Different cell passages were used as replicates. RNA-seq was performed in triplicates. Differentially expressed genes were defined by a padj < 0.05. Differentially spliced genes were defined by a p-value < 0.05 and a dPSI > 0.05.

Supplementary Table legends

Table S1: SRRM2 wt interactome.

Table S2: SRRM2 S1444P interactome.

Table S3: Differentially expressed genes S1444P vs wt.

Table S4: GO analysis of pathways enriched with differentially expressed genes.

Table S5: Splicing comparison S1444P vs wt.

Table S6: Phosphopeptides identified in SRRM2 wt and S1444P mass spectrometry.

Table S7: Antibodies used in this study.

Table S8: Oligonucleotides used in this study.